Materials Science & Engineering C 128 (2021) 112314

Contents lists available at ScienceDirect

Materials Science & Engineering C

journal homepage: www.elsevier.com/locate/msec

A new biocompatible silver/polypyrrole composite with *in vitro* antitumor activity

Elton Marlon de Araújo Lima [a,d,e], Vanderlan Nogueira Holanda [b,d], Gabriela Plautz Ratkovski [c,e], Welson Vicente da Silva [d], Pedro Henrique do Nascimento [d], Regina Celia Bressan Queiroz de Figueiredo [d,1], Celso Pinto de Melo [a,e,*,1]

[a] Pós-graduação em Ciência de Materiais, Centro de Ciências Exatas e da Natureza, Universidade Federal de Pernambuco, 50670-901 Recife, Pernambuco, Brazil
[b] Departamento de Bioquímica, Centro de Biociências, Universidade Federal de Pernambuco, Avenida Professor Moraes Rego, 1235, 50670-901 Recife, PE, Brazil
[c] Pós-graduação em Física, Centro de Ciências Exatas e da Natureza, Universidade Federal de Pernambuco, 50670-901 Recife, Pernambuco, Brazil
[d] Laboratório de Biologia Celular de Patógenos, Instituto Aggeu Magalhães, Departamento de Microbiologia, Avenida Professor Moraes Rego, 1235, 50670-901 Recife, Pernambuco, Brazil
[e] Departamento de Física, Centro de Ciências Exatas e da Natureza, Universidade Federal de Pernambuco, 50670-901 Recife, Pernambuco, Brazil

ARTICLE INFO

Keywords:
Polypyrrole
Metal nanoparticles
Biomaterials
Cytotoxicity

ABSTRACT

We used an *in situ* chemical oxidation method to prepare a new composite of silver nanoparticles (AgNPs) with polypyrrole (PPy), whose properties were optimized through a 2^3-factorial design of the synthesis conditions. The successful formation of the AgNPs/PPy composite was confirmed by UV–Visible and FTIR spectroscopies. Transmission electron microscopy revealed the presence of AgNPs smaller than 100 nm, dispersed into the PPy matrix. This hybrid composite exhibits a blue fluorescence emission after excitation in the ultraviolet region. In MTT assays, the AgNPs/PPy composite exhibited low cytotoxicity toward non-tumoral cell lines (fibroblast, Vero, and macrophages) and selectively inhibited the viability of HeLa cells. The AgNPs/PPy composite induces ultrastructural changes in HeLa cells that are consistent with the noticeable selectivity exhibited toward them when compared to its action against non-tumoral cell lineages. Also, the AgNPs/PPy exhibited a hemolytic activity below 14% for all blood groups tested, at concentrations up to 125 μg/mL. These results suggest that the AgNPs/PPy composite has a promising potential for use as an antitumoral agent.

1. Introduction

Conductive polymers (CPs) combine typical metallic properties, as elevated electrical conductivity and nonlinear optical properties, with an easy synthesis and flexibility in processing [1–3]. To a certain degree, their electrical properties can be controlled by chemical or electrochemical doping, *i.e.*, the oxidation or reduction of the main polymeric chain [4], which creates charged conformational defects [5,6]. These non-conventional polymers are usually conjugated systems, in which the induced defects exhibit high mobility along the backbone of alternating single and double covalent bonds. Furthermore, several CPs can present environmental stability and good compatibility with cells, tissues, and organs [7], allowing their use in different biological and material science applications [8].

Polypyrrole (PPy), in special, is a CP that has attracted great interest as a smart biomaterial due to their useful features such as good chemical stability and high conductivity under physiological conditions [8]. PPy has also been extensively investigated as an active agent in drug delivery systems, biosensors, neural interface, electrocatalytic platforms, and therapeutic protocols [9–12].

Composites of CPs with metal (gold, silver, iron oxide, *etc.*) nanoparticles have been shown to exhibit enhanced conductivity and interesting responses that have been exploited for the development of biological and material science applications [13–17]. Usually, the physicochemical properties of these hybrid nanostructures are remarkably different from their isolated components [18].

Good biocompatibility, *i.e.*, the ability to provide beneficial cellular or tissue response without causing deleterious collateral effects [8,19],

* Corresponding author at: Departamento de Física, Laboratório de Polímeros Não-Convencionais, Centro de Ciências Exatas e da Natureza, Av. Jorn. Aníbal Fernandes, s/n - Cidade Universitária, Recife - PE, 50740-540 Recife, Pernambuco, Brazil.
E-mail address: celso.melo@ufpe.br (C.P. de Melo).
[1] These authors contributed equally.

https://doi.org/10.1016/j.msec.2021.112314
Received 13 March 2021; Received in revised form 30 June 2021; Accepted 7 July 2021
Available online 14 July 2021

is an essential characteristic of any material with potential for use in biological applications [20,21]. The biocompatibility of PPy, which has been demonstrated in both *in vitro* and *in vivo* models [22], has allowed its use as a convenient substrate for the immobilization of biomolecules [23]. Due to their significant inhibitory activity on many species of bacteria [24,25], silver nanoparticles (AgNPs) alone exhibit a high antibacterial activity that has been exploited in medical applications and the development of commercial products [26]. However, it is well known that when used in their pristine form these particles can induce cell membrane damage and/or cause oxidative stress [27].

PPy-AgNPs composites have been used in the stabilization of oil-in-water emulsions [28] and as efficient nanocatalysts for the alkylation of amines [29]. It has been shown that the addition of AgNPs to a polymeric matrix can affect their interaction with cells and tissues [21]. Hybrid nanomaterials (such as polymer/metal nanoparticles) have been used in coatings with reduced toxicity and low level of particle aggregation [15,30], as well as antimicrobial agents [31,32] and platforms for cancer treatment [33]. Scanty information is available on the cytotoxic potential of hybrid composites based on PPy and AgNPs, and the evaluation of possible effects of AgNPs/PPy composites on mammalian cell systems remains an open field of investigation, with multiple avenues for multifaceted biomedical applications.

In this work, we report a novel synthesis of AgNPs/PPy composite by a single step *in situ* chemical oxidation of pyrrole monomers by silver cations. A 2^3-factorial design was applied for the optimization of the physicochemical properties (maximum fluorescence emission, mean zeta potential, and mean particle size) of the AgNPs/PPy. UV–Visible spectroscopy, Fourier Transform Infrared Spectroscopy (FTIR), and transmission electron microscopy (TEM) were used to characterize the composite obtained using the optimal experimental conditions. We assayed the biocompatibility/cytotoxicity of the AgNPs/PPy composite on fibroblast, macrophages, Vero cells, and Human Cervix Epithelioid Carcinoma (HeLa) cells and examined its possible hemolytic activity toward ABO blood groups. The ultrastructural changes induced in these cells after exposure to the AgNPs/PPy composite was also investigated by Scanning Electron Microscopy.

2. Materials and methods

2.1. Chemical

Ethanol PA (C_2H_5OH - Química Moderna, Brazil) was used as a solvent, and silver nitrate ($AgNO_3$ 99% - Sigma-Aldrich, USA) as a metal precursor. The pyrrole monomer 98% (C_4H_5N) and (3-Mercaptopropyl) trimethoxysilane 95% ($(HS(CH_2)_3Si(OCH_3)_3)$ – MPTS) were obtained from Sigma-Aldrich (USA). All reagents were used without further purification, except pyrrole, which was distilled under vacuum before use. Deionized water, was obtained by Millipore Synergy® Water Purification system (Merck, USA).

2.2. Synthesis of AgNPs/PPy composite

The synthesis of the AgNPs/PPy composite was carried out according to Santos et al. [34], with slight modifications. The reaction was performed in a round-bottom flask containing 10 mL of ethanol, followed by the addition of pyrrole monomer ($3{,}0 \times 10^{-2}$ mol/L), $AgNO_3$ solution ($8{,}1 \times 10^{-5}$ mol/L), and MPTS ($2{,}7 \times 10^{-2}$ mol/L). The resulting colloidal solution was maintained under vigorous stirring at 1000 rpm for 48 h, at room temperature. The dark AgNPs/PPy precipitate obtained was centrifuged at 10,000 ×*g* and washed successively with methanol and ultrapure Milli-Q water, and then dried in an oven at 70 °C for 24 h.

2.3. Fluorescence emission screening of AgNPs/PPy composite

We investigated the fluorescence spectrum of the AgNPs/PPy composite in the (360–590) nm emission range, at room temperature (23 °C), using a FluoroLog-3 spectrofluorimeter (Horiba, USA), under excitation in the (290–400) nm range. The excitation and emission slits had an opening of 2 mm, and 5 nm step sweeps were performed, using quartz cuvettes with a 1 cm optical path. The Spectra Lux program [35] was used to design a color coordinate graph in the RGB spectrum.

2.4. Optimization of the experimental condition of AgNPs/PPy composite by factorial design

A factorial experimental design method [36,37] was used to identify the main variables which have a key influence on the maximum fluorescence emission intensity (I_{max}), mean zeta potential (MZP), and mean particle size distribution (*Z*-Ave) of the AgNPs/PPy composite. The following variables were considered: (A) concentration of PPy monomers, (B) concentration of AgNPs, and (C) concentration of MPTS. A factorial design was implemented using two selected levels lower (−) and upper (+) for each variable (Table 1). By combining three-factor variables with the two levels for each one, 8 possible experiments (2^3) were performed in duplicate, resulting in a total of 16 experiments (Table S1). The significance of the effects of each variable was evaluated by the analysis of variance (ANOVA) using the statistical software Statistica 10 (Statsoft, USA). A p-value < 0.05 was used to indicate which variables were statistically significant, within a 95% confidence interval of Student's t distribution [38]. The statistical data were compared with Pareto chart analysis.

2.4.1. Z-average size and MZP measurements

The Z-Ave size and MZP of the sixteen AgNPs/PPy formulations were analyzed using a Zetasizer NANO-2590 (Malvern Instruments, UK). The Z-Ave were obtained by Dynamic Light Scattering (DLS) analysis, in which 10 μL of the AgNPs/PPy composite were previously dispersed in 1 mL of ethanol P.A.. A polystyrene cuvette with a 1 cm optical path was filled, capped, and checked for the absence of any bubbles. The measurements were performed with a laser ($\lambda = 633$ nm) under a spreading angle of 90° and a temperature of 25 °C. The zeta potential was assayed from the electrophoretic mobility of each one of the sixteen runs of the complete factorial design. The main zeta potential was calculated from the average of three values of the electrophoretic mobility of each one of the sixteen AgNPs/PPy composite formulations. All measurements were performed in a polystyrene cuvette with a 1 cm optical path, using an electrode for aqueous systems.

2.5. Characterization methods

2.5.1. UV–visible and FTIR spectroscopies

The absorption UV–Visible spectra of dilute AgNPs/PPy solutions (5:1000 *v*/v) were obtained in the 200–1000 nm range, by using a quartz cell with an optical length of 1.0 cm, in a UV-2600 spectrophotometer (Shimadzu, Japan). The FTIR spectra were recorded on an FTIR-ATR spectrophotometer 4600 (Jasco Corporation, Japan) equipped with an ATR attachment comprising a ZnSe crystal with a central incidence angle of 45°, a circular contact area of 4.9 mm^2 and operating at a resolution of 4 cm^{-1} in the 4000 cm^{-1} to 400 cm^{-1} range.

Table 1
Experimental factors and levels in the 2^3-factorial design for the AgNPs/PPy composite synthesis optimization.

Factors	Levels (mol/L)	
	Lower (−)	Upper (+)
MPTS	$1{,}6 \times 10^{-2}$	$2{,}7 \times 10^{-2}$
Pyrrole	$1{,}4 \times 10^{-2}$	$3{,}0 \times 10^{-2}$
$AgNO_3$	$3{,}6 \times 10^{-5}$	$8{,}1 \times 10^{-5}$

MPTS: (3-Mercaptopropyl)trimethoxysilane.

2.5.2. Transmission electron microscopy

The structural characterization of the AgNPs/PPy composite was carried out using an FEI Tecnai Spirit transmission electron microscope (FEI, USA) operating at 120 kV. For this, we dropped 10 μL of diluted AgNPs/PPy solution on a 400-mesh carbon-coated copper grid that was allowed to dry completely, at room temperature, before obtaining the TEM images.

2.6. In vitro biocompatibility of AgNPs-PPy composite

2.6.1. Cell culture and cytotoxicity assay

For the biocompatibility studies, we used four mammalian cell lineages: J774A.1 macrophage (ATCC® TIB-67™), Vero (ATCC® CCL-81™), fibroblast (ATCC® PCS-201-012™), and HeLa (ATCC® CCL-2™). The Vero cells and macrophages (5×10^5 cells/well) were cultured in 96-well plates containing 100 μL of an RPMI 1640 medium (Sigma-Aldrich, USA) supplemented with 10% fetal bovine serum (FBS) and 1% penicillin-streptomycin solution (Sigma-Aldrich, USA). The fibroblasts and HeLa cells were cultivated at the same conditions for the macrophages and Vero cells, except by the use of a DMEM medium (Sigma-Aldrich, USA). After the adhesion, the cells were incubated in the appropriate culture medium in the absence (untreated control cells) or presence of different concentrations (31.2–500 μg/mL) of AgNPs/PPy composite for 24 h. After the incubation time, the cells were washed and reincubated in a fresh RPMI culture medium without phenol red (Sigma-Aldrich, USA), containing 5 mg/mL of 3-(4,5-Dimethyl-2-thiazolyl)-2,5-diphenyl-2H-tetrazolium bromide (MTT) (Sigma-Aldrich, USA) and cultivated for an additional period of 3 h at 37 °C. Afterward, the cells were solubilized in 100 μL of an acidified isopropanol solution (0,04 M HCl + absolute isopropanol), to dissolve the formazan dye. The absorbance was read in a microplate spectrophotometer (Bio-Rad®, California, USA) at 540 nm. Each analysis was performed in quadruplicate, in two independent experiments.

2.6.2. Ultrastructural analysis

The scanning electron microscopy (SEM) analysis was performed to investigate the effects of AgNPs/PPy on the morphology of HeLa and J774A.1 macrophage cells. For this, the HeLa and macrophages cells were treated with the AgNPs/PPy composite solutions at CC_{50} or 2× CC_{50} concentration, for 24 h. Untreated cells were used as a negative control. After incubation time, both the control and treated cells were washed with PBS and fixed for 2 h at room temperature in a solution containing 2.5% glutaraldehyde/4% paraformaldehyde in 0.1 M of cacodylate buffer at pH 7.2. After washing in the same buffer, the cells were post-fixed for 1 h with 1% osmium tetroxide/0.8% potassium ferricyanide/5 mM $CaCl_2$ diluted in 0.1 M cacodylate buffer solution at pH 7.2. The samples were dehydrated in an increasing gradient series of ethanol, drying by critical point, covered with a 20 nm thick gold layer, and analyzed in a JEOL T-200 scanning electron microscope (JEOL, Japan).

2.6.3. Hemolytic assay

The hemolytic activity of AgNPs/PPy composite was investigated on human erythrocytes (A, B, O, and AB), according to the protocol established by Yang et al. [39]. Briefly, erythrocytes of each blood type were serially diluted in saline (NaCl 0.9%) and incubated in a 96-well microplate, in the presence of AgNPs/PPy solution at different concentrations (31.2–500 μg/mL), for 30 min at 37 °C. After incubation, the microplates were centrifuged at 1500 ×*g* for 4 min, and the hemolysis activity was quantified in a UV–Vis spectrophotometer at 412 nm. Erythrocytes incubated in 100 μL of saline solution (NaCl 0.9%) or treated with 100 μL of Triton X-100 (0,1%) were used as a negative and positive control of hemolysis, respectively. The hemolysis rate was determined as

$$\%_{hemolysis} = \frac{A_s - A_N}{A_p - A_N} \times 100,$$

where A_S, A_P, and A_N are the absorbances of the tested sample, the positive (100% of lysis), and the negative control, respectively. Each analysis was carried out in three independent experiments in triplicate.

2.7. Ethical considerations

The present study was carried out following the ethical principles adopted by the Brazilian Law 11.794/2008 and National Research Ethics Committee (CEP/CONEP), under the number CAAE: 06959119.8.0000.5048.

2.8. Statistical analysis

The statistical analyses were performed using the SPSS Statistics for Windows (Version 18.0. IBM Corp. USA). The 50% cytotoxic concentration (CC_{50}) was calculated by linear regression. All data are presented as the average value ± standard deviations. A value of $p < 0.05$ was considered as statistically significant by one-way ANOVA test, and Dunnett's Post-test in GraphPadPrism 5.0 (Graphpad, California, USA).

3. Results and discussion

3.1. Synthesis of the AgNPs/PPy composite

In this work, the AgNPs/PPy composite was obtained efficiently and economically through a one-pot reaction. A schematic diagram and the mechanism proposed for the colloidal formation of AgNPs/PPy are depicted in Fig. 1, according to Oliveira et al. [40]. Initially, the silver precursor ($AgNO_3$) dissociates into silver cations (Ag^+) and nitrate anions (NO_3^-) (Step a). Consequently, the Ag^+ cation acts as an oxidizing agent for the *in situ* chemical polymerization of the pyrrole monomers, resulting in the simultaneous formation of pyrrole radical cation and metallic silver (Ag^0) (Step b). The PPy molecules are absorbed by hydrogen bonding and electrostatic interaction onto the mercaptocarboxylic acid, capping the AgNPs [41,42]; the silver nanoparticles are aggregated inside the PPy chains (Step c) [28,40,43,44]. The MPTS is widely used to prevent the agglomeration of the formed nanoparticles, due to its chemical affinity – which is associated with the presence of thiol groups – toward different noble metals [45,46].

3.2. Fluorescence measurements and optimization of the experimental condition of AgNPs/PPy composite

Highly fluorescent nanoparticles, as conductive polymers, have attracted scientific and industrial interest due to their remarkable optical/fluorescence properties, which can be exploited in various applications such as high-throughput screening, ultrasensitive assays, live-cell imaging, and photodynamic therapy [47]. Previous work conducted by our group demonstrated that the interaction between the metal particles and the polymeric chains in the AuNPs/Polyaniline composite results in remarkable fluorescence emission in the visible region [34]. To investigate the photoluminescence of the as-prepared AgNPs/PPy, an excitation and emission spectrum screening was performed (Fig. 2A–B). The maximum fluorescence emission intensity (I_{max}) was observed at ~425 nm (Fig. 2B), for a $\lambda_{exc} = 350$ nm (Fig. 2A). This corresponds to the blue region in the visible spectrum, as confirmed by the corresponding color coordinate graph (Fig. 2C). Dong et al. [47] have reported a fluorescence emission peak around 440 nm for PPy nanospheres excited at 360 nm. The interaction of the AgNPs with PPy chains can account for the blue-shift observed in our case. Ramanavicius et al. [48] showed that quantum dots covered with PPy layer presented enhanced photoluminescence and resistance to the photobleaching. It has been reported

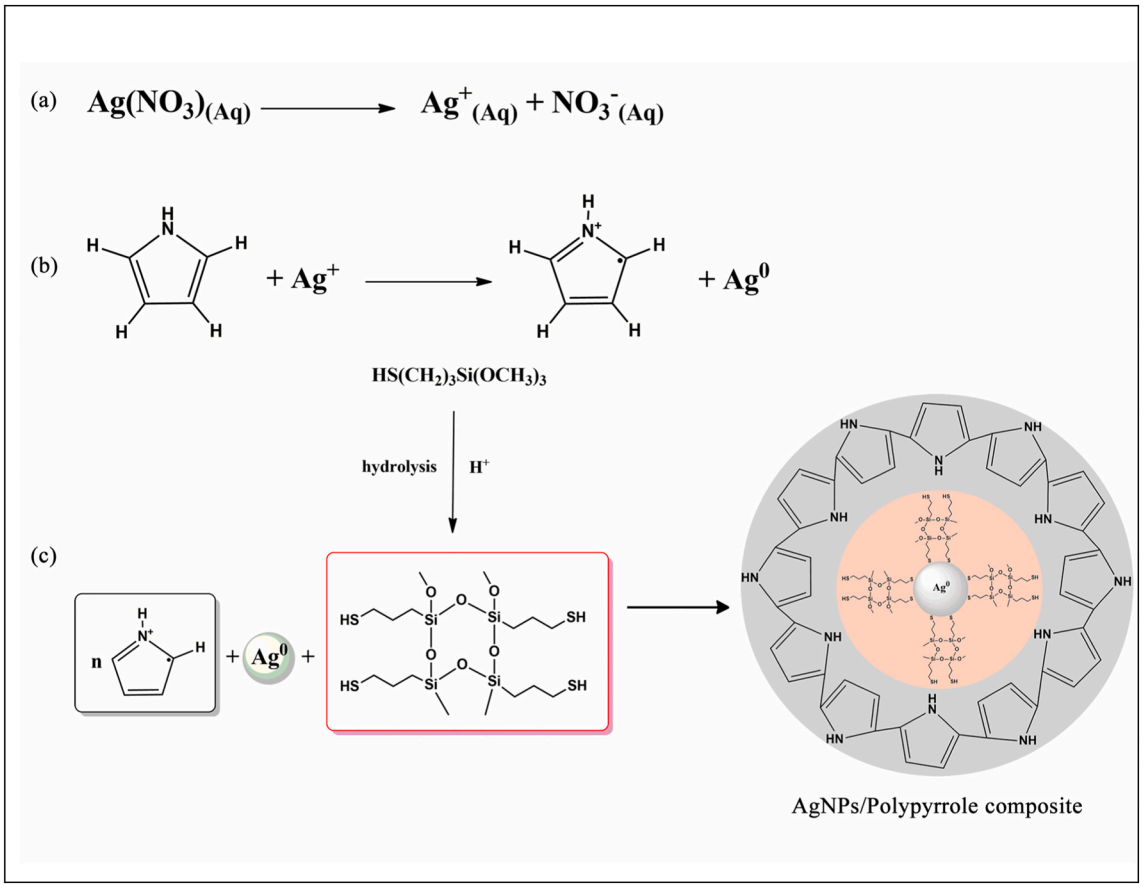

Fig. 1. Mechanism proposed for the of AgNPs/PPy composite formation.

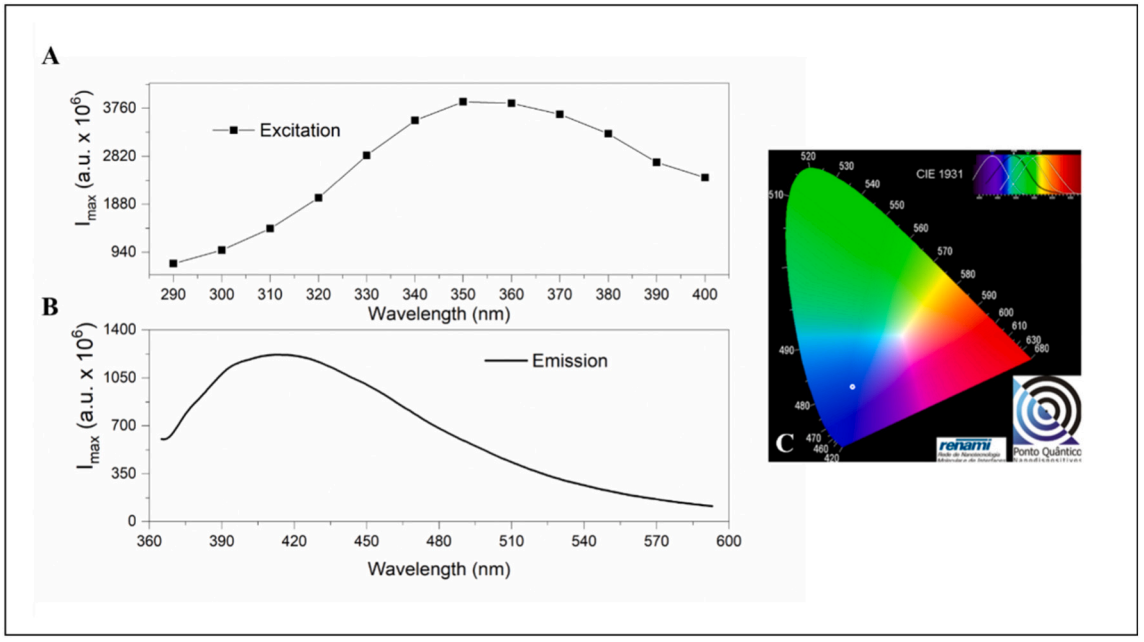

Fig. 2. Fluorescence intensity of the AgNPs/PPy composite at excitation wavelengths at 290–400 nm excitation wavelengths range (A), fluorescence emission spectrum (λ_{exc} = 350 nm) (B), and color coordinate in the RGB spectrum (C).

that besides playing an important role in modulating the fluorescence of dyes, noble metals as gold and silver can become fluorescent *per se*, when their size is sharply decreased to the subnanometer range and/or they are stabilized with appropriate ligands [49]. The fluorescence emission of the AgNPs/PPy composite may result from the interaction between the pyrrole monomers and the AgNPs formed during the AgNPs/PPy

synthesis process [34,50].

Because the existence of fluorescence expands the diversity of biological applications of the AgNPs/PPy composite, we further investigated the influence of the concentrations of Ag, pyrrole monomers, and MPTS (independent variables) on the maximum emission fluorescence intensity (I_{max}, under 350 nm excitation), mean zeta potential (MZP), and the mean particle size distribution (*Z*-Ave) using the 2^3-factorial design. This approach also allowed us to choose the optimal conditions for the synthesis of AgNPs/PPy that would better fit the physicochemical parameters evaluated. A matrix consisting of the selected variables (concentration of pyrrole, AgNPs, and MPTS) together with the corresponding responses (I_{max}, Z-ave, and MZP) is presented in Table 2.

The Pareto chart analysis showed which of three variables analyzed (concentration of MPTS, $AgNO_3$, and pyrrole) or its interactions should be statistically significant based on the variation between the two levels chosen. The red line at 0.05 indicated the statistical significance (Fig. 3). Our results demonstrated that the I_{max} is increased when the AgNPs/PPy composite was synthesized with the highest concentration of pyrrole and $AgNO_3$ (Fig. 3A), as indicated by the positive value of the standardized effect ($AgNO_3$ = 7.73; pyrrole = 3.51; Ag and Pyrrole interaction = 2.77). The positive interactions between these variables were confirmed by the analysis of variance (ANOVA) (Table S2).

The MZP, which depends on the surface charge, plays a key role in the stability of nanoparticles in suspension and is an important parameter for the synthesis and functionality of solid-state and soft matter synthetic colloids [51]. The analysis of the MZP measurements showed negative absolute values, for all 16 samples tested indicating a able colloidal dispersion of AgNPs/PPy composite (Table 2). As shown in the Pareto chart (Fig. 3B), the concentration of MPTS, as expected, was the variable that presented the most significant influence on MZP, as also demonstrated by the ANOVA analysis (Table S2). When MPTS, used in its lower level (−), was combined with the upper levels (+) of $AgNO_3$ and pyrrole there is a reduction in the average value of the main zeta potential (run 7 and 8; and run 15 and 16, respectively). When the amount of PPy was increased, the MZP was more negative (run 7 and 8; and run 15 and 16, respectively). Wen et al. [52] have found that the zeta potential of PPy/Ag composites becomes more negative when the relative amount of PPy is increased, as a result of a stronger interaction between the PPy chains and AgNPs.

The influence of reagent concentrations on *Z*-Ave was also analyzed. The Z-ave measurements of the samples (1–16 runs) showed that the size of the composite is influenced by reagent concentration, varying from 971.30 nm for MPTS (+), pyrrole (−), and $AgNO_3$ (+) to 942.70 nm for MPTS (+), pyrrole (+) and $AgNO_3$ (+) (run 14 and 16). The Pareto chart demonstrated that pyrrole concentration has the highest standardized effect on this parameter (3,42) at a 95% confidence level (Fig. 3C). This result indicates that only the pyrrole concentration was statistically significant and the best response for the dispersion of the average particle size occurred when this variable was at its upper level (+). The positive effect showed on the Pareto chart also corroborates with the main effect of pyrrole concentration (statistical test - Table S2) that was observed for I_{max}.

Taking into account the observed influence of the concentration of composite constituents on the I_{max}, MZP, and Z-ave, the optimal condition for the synthesis of colloidal formulation of AgNPs/PPy was those where MPTS (−), $AgNO_3$ (+), and pyrrole (+). In this regard, this optimized formulation was used for the subsequent characterizations and the investigation of its biocompatibility and antimoral activity.

Table 2
Matrix of interactions and results of the complete factorial design of the synthesis of AgNPs/PPy composite. Response: higher emission intensity (I_{max}) recorded at λ_{exc} = 350 nm, mean zeta potential (MZP), and the mean particle size (Z-Ave).

Run	Variables			Responses		
	MPTS	Pyrrole	$AgNO_3$	I_{max} (a.u)	MZP (mV)	Z-Ave (nm)
1	−	−	−	4.62×10^5	−25.7	843.20
2	+	−	−	3.50×10^5	−38.9	764.10
3	−	+	−	6.42×10^5	−19.2	798.70
4	+	+	−	7.72×10^5	−21.6	823.70
5	−	−	+	3.92×10^5	−22.3	950.00
6	+	−	+	5.64×10^5	−44.1	896.20
7	−	+	+	1.14×10^6	−33.1	851.30
8	+	+	+	1.12×10^6	−43.9	867.20
9	−	−	−	6.97×10^5	−38.9	892.60
10	+	−	−	4.99×10^5	−38.4	843.90
11	−	+	−	8.58×10^5	−25.9	864.10
12	+	+	−	8.61×10^5	−36.4	795.70
13	−	−	+	6.48×10^5	−32.6	885.70
14	+	−	+	5.73×10^5	−45.0	971.30
15	−	+	+	1.22×10^6	−44.1	964.60
16	+	+	+	1.08×10^6	−46.4	942.70

3.3. Spectroscopic and structural characterization of the Ag/polypyrrole composite

The absorption spectrum of the AgNPs/PPy composite is shown in Fig. 4. It has been verified that the predicted optimal point of the AgNPs/PPy has two absorption bands at 230 nm and 280 nm, corresponding to the π-π* transitions of the benzenoid rings and the π-π* transitions of the pyrrole rings, respectively [47]. The shoulder at 470 nm (Fig. 4, inset) is associated with the overlapping of the π-π* transitions of the PPy and the presence of plasmons resonance surface of metallic nanoparticles [53]. Although the AgNPs commonly exhibit plasmon resonance bands in the (410–440) nm region [54], a band shift should be expected upon their incorporation into the polymeric chains [55,56].

The FTIR spectrum of the synthesized AgNPs/PPy composite confirmed the successful polymerization of pyrrole and the incorporation of the AgNPs (Fig. 5), even though some peaks become slightly displaced due to the interaction of the metallic nanoparticles with the PPy chains [42,57–59]. Characteristic peaks of PPy were observed in 1329 cm^{-1}, 1044 cm^{-1}, 879 cm^{-1}, and 601 cm^{-1}, which can be attributed respectively to the C═C stretch in the ring, C—H twist of the ring outside the plane, stretching of C═C, and deformation of C=C–N–H of the ring outside the plane [60]. The peak attributed to the pyrrole oxidation appears near 1379 cm^{-1} [61]. The peak at 1660 cm^{-1} is characteristic of the C═C bond stretch or can be assigned to the O=C–NH_2 groups. The peak around 1086 cm^{-1} can be assigned to the vibrations of the pyrrole ring [42,44,62].

The structural analysis of the AgNPs/PPy composite by TEM revealed the presence of both monodisperse and aggregated regions. In the monodisperse structures, the electron-dense core, which corresponds to single spherical silver nanoparticles with sizes smaller than 100 nm, is surrounded by an amorphous electron-lucent PPy matrix (Fig. 6A and B). On the other hand, the aggregates corresponded to a large polymeric matrix containing various inner silver nanoparticles, with sizes ranging from 200 nm to 500 nm (Fig. 6C and D). These agglomerate structures could have been formed by the concomitant reduction of silver cations and the growth of the PPy chains, which explains the higher mean particle size values obtained by DLS (Section 3.2).

3.4. Cytotoxic assay on mammalian cells

The biocompatibility of a given material can be assessed by examining the subsequent viability of selected cells exposed to it [20,63]. In this work, the cytotoxicity of as-prepared AgNPs/PPy composite was examined by performing MTT assays on fibroblasts, macrophages, and Vero cells at different concentrations of the composite. While fibroblasts and Vero Cells are frequently used for the evaluation of the cytotoxicity of biomaterials [20,64], macrophages are immunocompetent cells that first interact with foreign particles, efficiently phagocytizing them [65]. Macrophages also participate in the immune response to cancer cells [66]. Human cervix epithelioid carcinoma (HeLa) cells have been

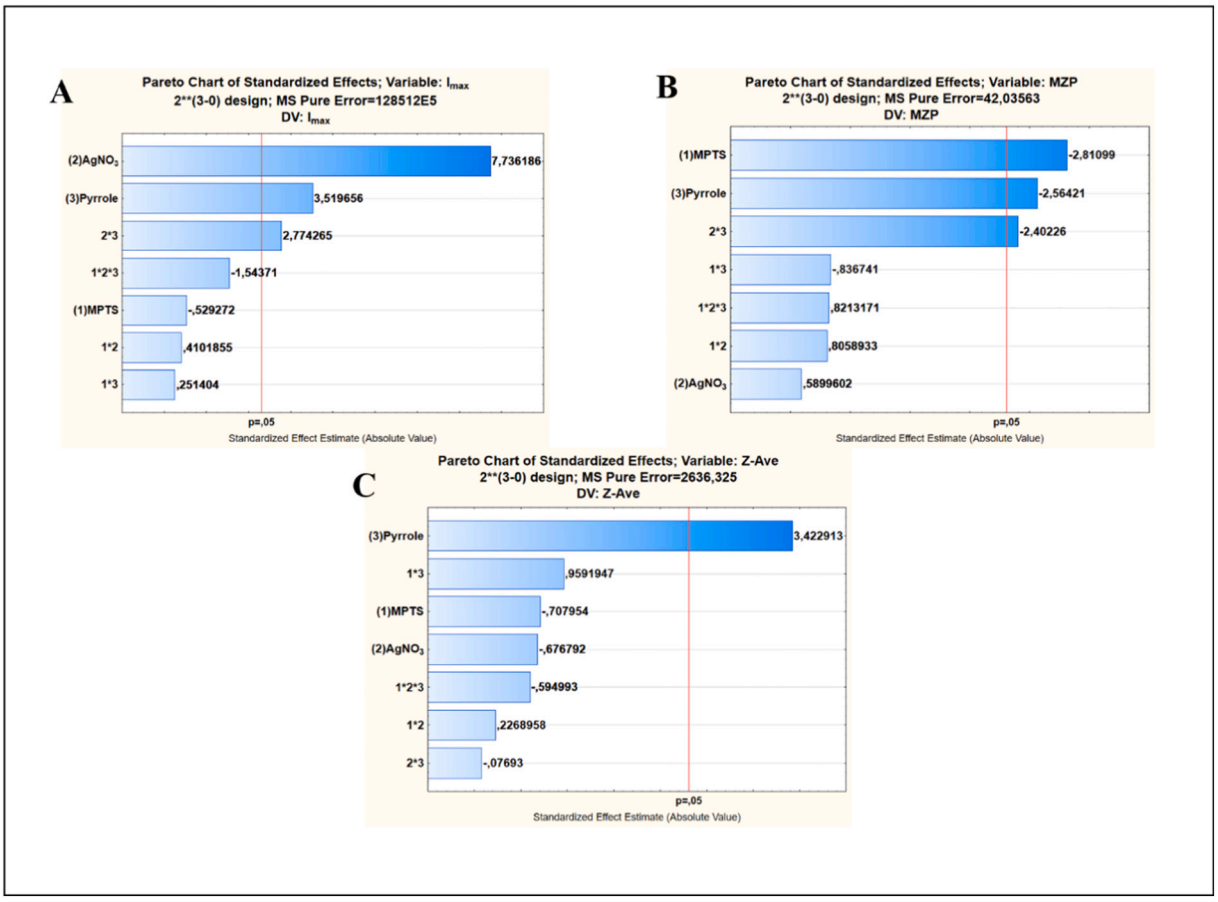

Fig. 3. Pareto chart of the effect of MPTS, $AgNO_3$, and pyrrole concentration and on Imax (A), MZP (B), and Z-Ave (C) of AgNPs/PPy composite. The vertical red line in the Pareto chart indicates the significant effects at a 95% confidence level. (For interpretation of the references to color in this figure caption, the reader is referred to the web version of this article.)

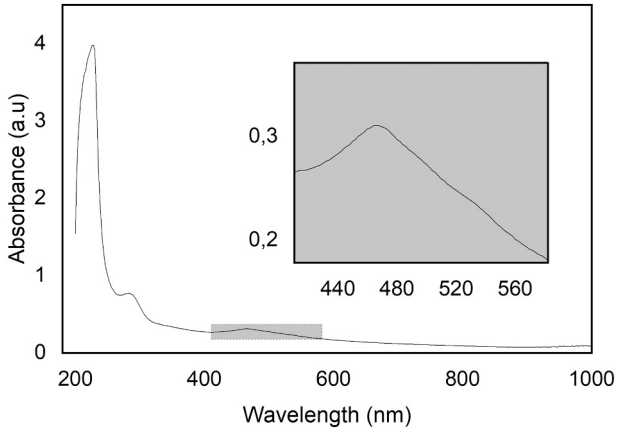

Fig. 4. UV–Visible spectrum of the AgNPs/PPy composite.

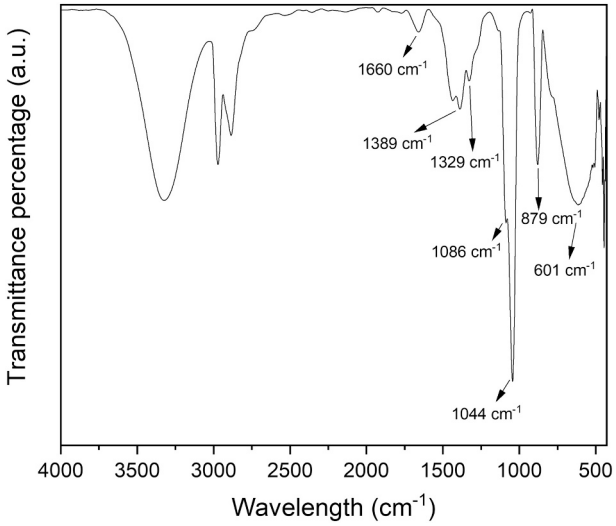

Fig. 5. FTIR spectrum of the AgNPs/PPy composite.

efficiently used as a model to evaluate the antitumor activity and tumor targeting of hybrid nanomaterials [67]. As a manner to assess the possible role of the AgNPs/PPy composite on cancer therapy, we evaluated its effect on HeLa cells.

Our results indicated that the AgNPs/PPy composite did not induce significant cytotoxic activity on macrophages and fibroblast and Vero cells (Fig. 7A–C). The corresponding CC_{50} could not be estimated by regression analysis, and so it was considered greater than the highest concentration tested (500 μg/mL) in these cells (Table 3). Our results are consistent with the good biocompatibility already reported in the literature for PPy-based molecules [68–70]. It has been demonstrated that PPy was not toxic to mouse marrow-derived stem cells and sustain the attachment and proliferation of these cells on the PPy-modified surfaces. It has been also shown that the presence of amine groups and positive charges in the PPy structures allows the adhesion and proliferation of fibroblasts and other adherent cells [70–72]. Our results

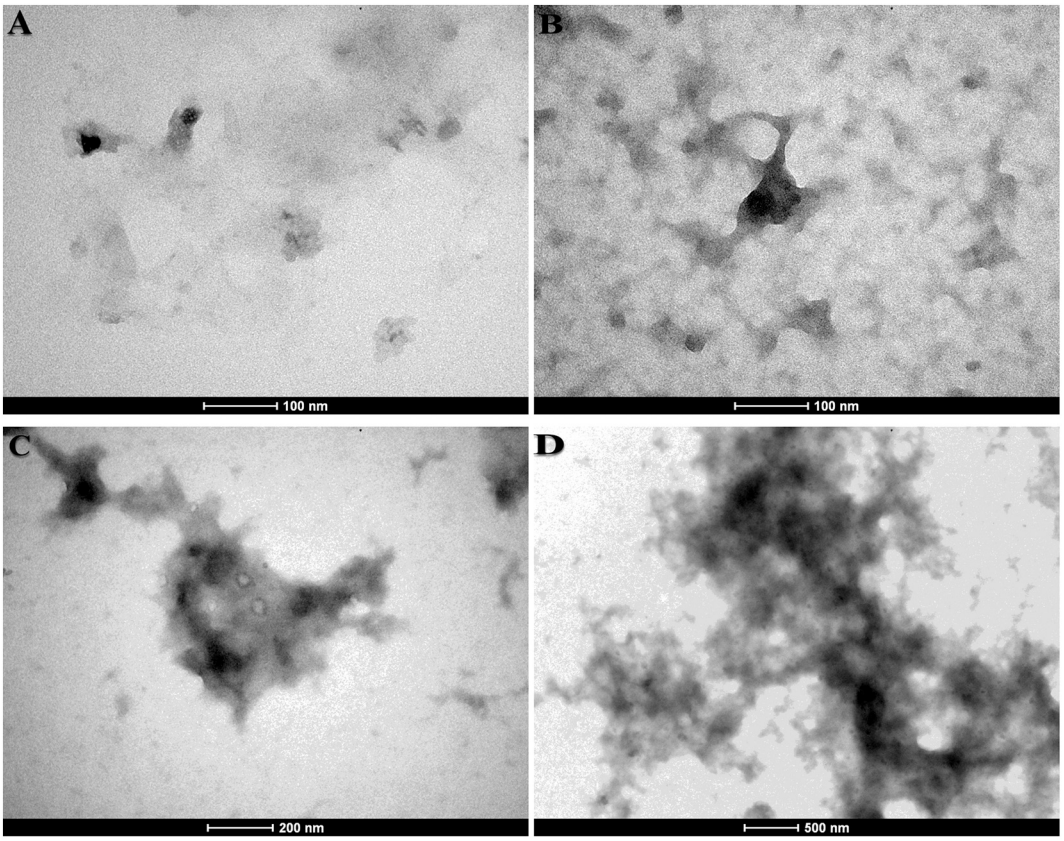

Fig. 6. TEM of the AgNPs/PPy composite in monodisperse shapes (A and B) and its agglomerated morphology (C and D).

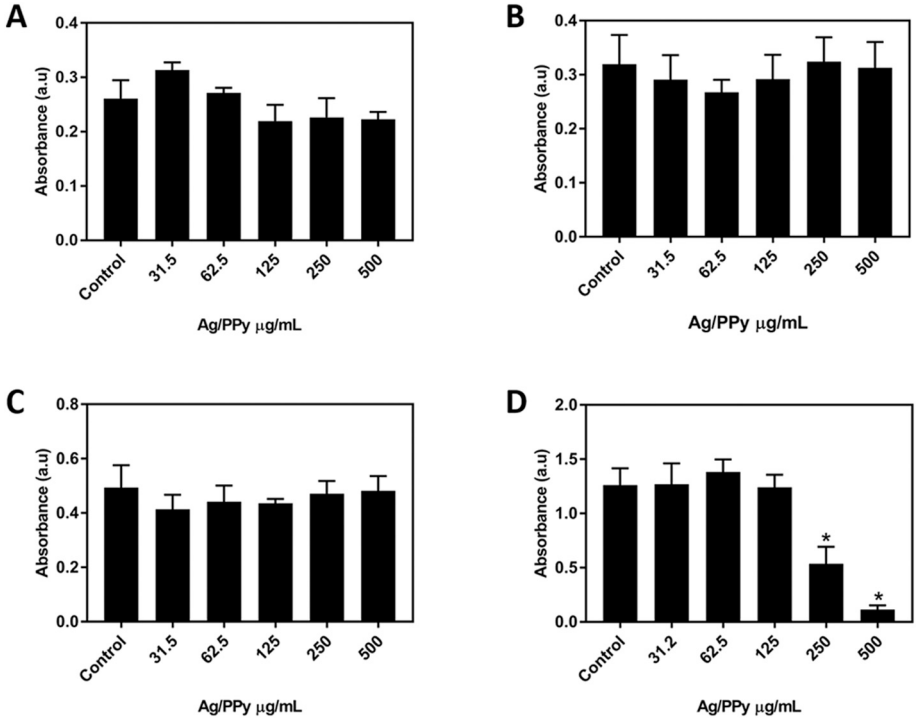

Fig. 7. Effect of the AgNPs/PPy composite on mammalian cells: (A) fibroblasts, (B) Vero, (C) J774A.1, and (D) HeLa. Values represent the mean ± standard deviation of three independent experiments in triplicate. *Significant differences at $p < 0.05$ compared to untreated control.

Table 3
The effect of AgNPs/PPy on the viability of mammalian cells.

Cell line	CC_{50} (μg/mL)
Fibroblast	>500
Vero	>500
Macrophage (J774A.1)	>500
HeLa	210,06

CC_{50} – concentration (μg/mL) able to decrease the cell viability by 50%.

indicated that while the viability of fibroblasts cultivated in presence of the lowest concentration of AgNPs/PPy slightly increases (Fig. 7A), a significant decrease in the viability of HeLa cells treated with 250 and 500 μg/mL of the composite occurs. For the highest concentration tested, the inhibition of cell viability was close to 90%. The estimated CC_{50} for HeLa cells after 24 h of incubation was 210 μg/mL (Table 3). The action of PPy-based materials on the viability of cancer cells has already been pointed out [73]. However, most of the previous works have been limited to the use of such materials as active agents for photothermal therapy or as biosensors for cancer diagnosis [7,15,74,75]. To the best of our knowledge, the present results correspond to the first report of the antitumoral activity of AgNPs/PPy composite *per se*.

3.5. Effect of AgNPs/PPy composite on the ultrastructure of mammalian cells

We used scanning electron microscopy to investigate the effects of the AgNPs/PPy composite on the morphology of J774A.1 macrophages and HeLa cells. To establish a baseline for comparison, in Fig. 8A and B we present the characteristic morphology of untreated J774A.1 macrophages and HeLa cells. The control macrophages, which present round to flattened shapes, were found to firmly attach to the substrate. Prominent filopodia and lamellipodia projections are commonly observed in these cells (Fig. 8A). The HeLa cells presented flattened and/or polygonal morphology. The cell surface of these cells is decorated with numerous microvilli (Fig. 8B) [76–78]. The surface topography of both types of cells indicates that they are extraordinarily active [79]. No damage to the plasma membrane was observed when the J774A.1 macrophage was treated with CC_{50} of the AgNPs/PPy composite (Fig. 8C). However, under this treatment condition, these cells became more flattened and with longer pseudopodia compared to non-treated cells (Fig. 8C). This phenotype has been usually associated with macrophage activation [80,81]. The treatment of macrophages with LPS, which is a standard activator of macrophages toward classical M1 activation profile, quickly induces the formation of pseudopods, filopodia-like projection, and the spreading of these cells on the substrate, in a similar way to those observed in our study [82]. Similarly,

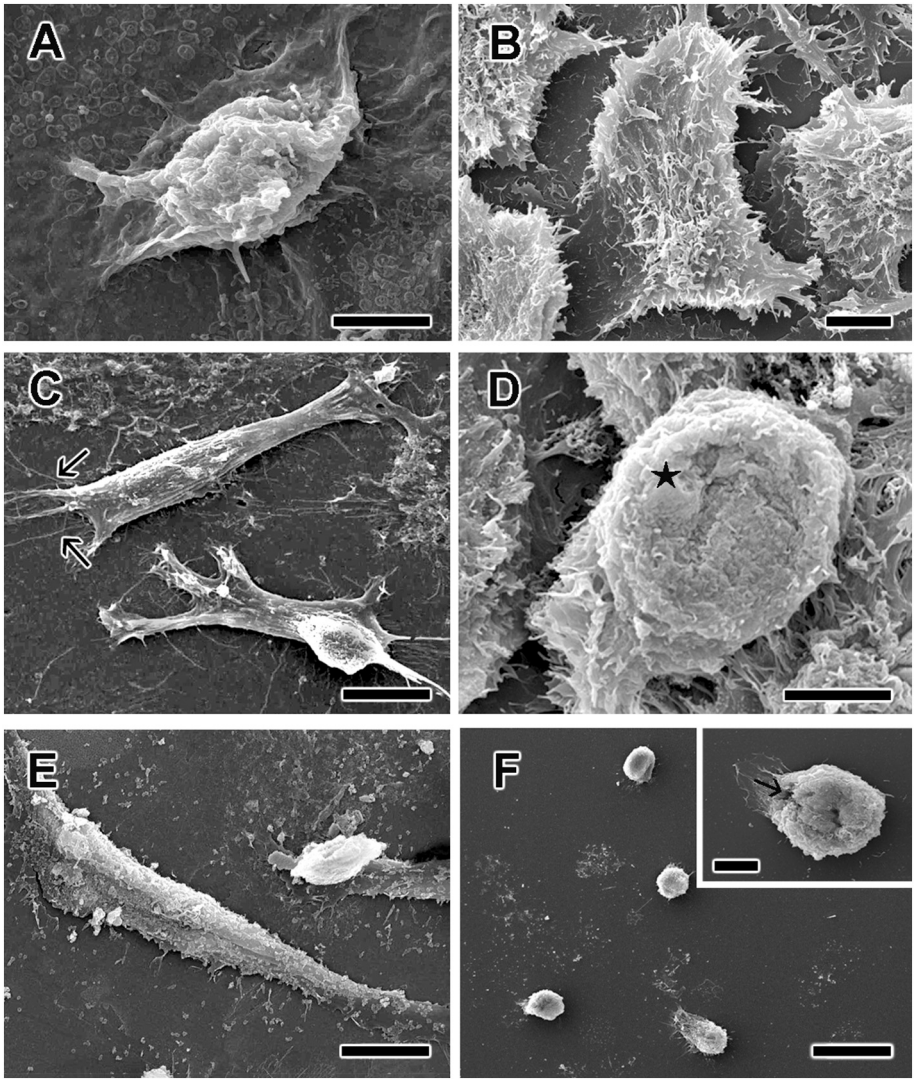

Fig. 8. Representative micrographs of the effects of AgNPs/PPy on the morphology of macrophages (left column) and HeLa cells (right column). (A) Untreated macrophages presenting a round shape and evident filopodia and lamellipodia tightly attached to the substrate with a clear emission of filopodia and lamellipodia. (B) Untreated HeLa cells presenting flattened morphology. The cell surface showed characteristic microvilli extending from the cell surface. (C–D) Cells treated with CC_{50} of AgNPs/PPy. (C) treated-macrophages showing spread and flattened morphology with long filopodia projections (black arrow) (D) Detail of a HeLa cell showing a rounding of the cell body and loss of microvilli (black star). (E–F) Macrophages (E) and HeLa cells (F) were treated with 2 × IC_{50} of AgNPs/PPy (F). Detail of HeLa cell culture showing scant adhered cells, all of them with a round morphology. Note the presence of membrane perforations (black arrow) and loss of microvilli structures (inset). Bars: A, B and D = 2 μm; C, E, =5 μm; F = 10 μm; inset = 1 μm.

Gniadek et al. [83] demonstrated that THP-1 monocytes in contact with PPy-coated materials, including AgNPs/PPy, showed numerous funnel-like lamellipodia characteristics of macrophage activation. Classically activated M1-polarized macrophages have an important role in refocusing the immune system for the elimination of cancer. Thus, the AgNPs/PPy composite may induce the polarization of macrophages toward the M1 phenotype, making them more competent to attack and phagocyte tumor cells [80,84].

The treatment of HeLa cells with CC_{50} of AgNPs/PPy composites induced the loss of microvilli, whereas their plasma membrane assumes a corrugated appearance (Fig. 8D). These morphological changes are indicative of a loss of plasma membrane function. Only at the higher concentration tested, the AgNPs/PPy composite induced some damage to the macrophage membrane (Fig. 8E), and, even so, to a lesser extent than the damage caused to the HeLa cells. In all concentrations tested, the morphology of the HeLa cells assumed a more globular aspect, with damage to the plasma membrane being observed even at the lowest AgNPs/PPy concentration tested (Fig. 8D and F). Hence, our results indicate that the AgNPs/PPy composite selectively affects the HeLa cells relative to the treated fibroblast, Vero cells, and macrophages.

It is usually assumed that the antitumor activity of AgNPs is mainly due to the possible release of metallic silver (Ag^0) and silver ions (Ag^+), which can trigger increased ROS production leading to oxidative stress, DNA, mitochondrial and membrane damage, genotoxicity, resulting in cell death by necrosis or apoptosis [85]. Consistently, our morphological results showed that the treatment of HeLa cells with the composite caused damage to the plasma membrane and the presence of cellular debris, characteristic of necrosis. It has been demonstrated that reactive oxygen species (ROS) have a paradoxical role in cancer. ROS can promote protumorigenic signaling, favoring cancer cell proliferation, survival, and adaptation to hypoxia [86]. On the other hand, ROS can induce antitumorigenic signaling and trigger oxidative stress-induced cancer cell death [87,88]. The high metabolic activity in cancer cells, needed for cell transformation and tumorigenesis, increases ROS production by these cells. Concomitantly, to maintain ROS homeostasis, tumor cells altered their antioxidant capacity increasing their susceptibility to ROS-induced oxidative stress as compared to normal cells. Our results indicate that the combination of AgNPs with PPy chains has a noticeable effect on HeLa cells, without causing substantial damage to normal mammalian cells (macrophages, fibroblasts, and Vero cells). These results suggest that the presence of the PPy chains reduced the cytotoxic potential of AgNPs on non-tumoral cell lines. Despite the good biocompatibility of PPy to mammalian cells have been already reported in the literature, we cannot rule out that this CP also contributes, at least in part, to the cytotoxicity of AgNPs/PPy toward HeLa cells. Vaitkuviene et al. [72] showed that PPyNPs presented considered cytotoxic effects to the Jukart, MH-22A tumoral linages whereas the cytotoxic effect of these nanoparticles on primary mouse embryonic fibroblast was observed only at higher concentrations.

3.6. Hemolytic assay

The hemolytic activity is an important parameter to be considered when assessing the biocompatibility of a given material [89]. The hemolysis corresponds to the breakdown or destruction of the plasma membrane of Red Blood Cells (RBCs), with the subsequent release of hemoglobin [90]. A significant RBC rupture in response to the exposure to a material is an adverse effect that could lead to important pathological conditions, limiting its systematic use in medical devices and applications [91]. We used RBCs from the A, B, AB, and O human blood groups to investigate the hemolytic potential of the AgNPs/PPy composites (Fig. 9). The hemolytic activity of AgNPs/PPy composites was less than 20%, for all blood groups tested, at concentrations up to 125 μg/mL, which is a threshold value to consider a biomaterial as non-hemocompatible [62,92,93].

It is important to note that the composition of the human erythrocyte plasma membrane varies according to the blood group [94], leading to differences in the susceptibility of these cells to biomaterials [95,96]. Membrane proteins contribute considerably to the total surface charge of these cells. Particularly, the intermolecular interactions of composite materials with the surface of the different blood groups erythrocytes can modify the zeta potential of these cells [97–99]. It is worth mentioning that isolated silver nanoparticles can induce the rupture of the erythrocyte membrane [15,91,95]. The cytotoxic and hemolytic effects of AgNPs or silver-based nanocomposites on mammalian cells have been reported by various groups [91,100,101]. The hemolytic activity of isolated AgNPs seems to depend on their surface/volume ratio, with nanoparticles presenting a higher hemolytic activity than micron-size particles. On the other hand, as a hemocompatible material [22], PPy can protect the erythrocytes from the deleterious effects of Ag nanoparticles.

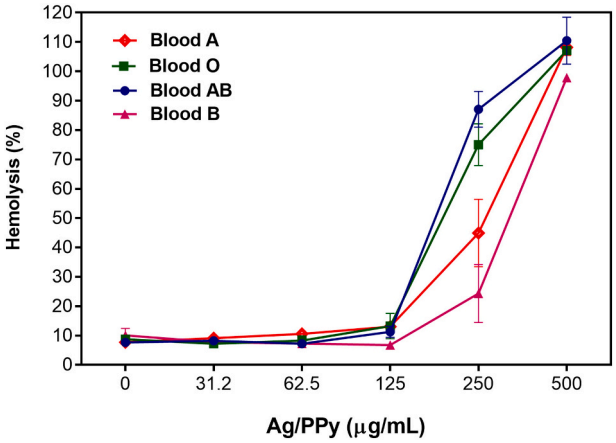

Fig. 9. Hemolytic percentage of AgNPs/PPy in different human erythrocytes groups.

4. Conclusions

We presented an easy method of preparing AgNPs/PPy composite which emits a fluorescent signal in the blue region of the visible spectrum, characterizing them by UV–Visible and FTIR spectroscopies, and TEM analyses. The impact of the concentration $AgNO_3$, pyrrole, and MPTS on the maximum fluorescence intensity, main zeta potential, and *Z*-Ave size was demonstrated by factorial design methodology and validate by statistical analysis (Pareto charts and ANOVA). This approach allowed us to optimize the experimental condition for the synthesis of AgNPs/PPy composite. We have shown that the optimized AgNPs/PPy composite exhibits low cytotoxicity toward non-tumoral cell lineages but has highly selective action against HeLa cells, in which severe membrane damage is induced, as observed by SEM. The AgNPs/PPy composite also exhibited a low hemolytic activity, when used at concentrations below 125 μg/mL. Overall, these results confirm the good biocompatibility and promising potential of the AgNPs/PPy composites as cytotoxic agents against HeLa cells without induces damage to healthy cells. Additionally, the fluorescence of these composites opens up the possibility of their use as biomarkers for diagnosis and biosensing. We believe that further studies are necessary to elucidate the mechanism of action of the AgNPs/PPy composite on HeLa cells, as well as on other tumoral cells both *in vitro* and *in vivo*.

CRediT authorship contribution statement

Elton Marlon de Araújo Lima: Conceptualization, Methodology, Formal analysis, Investigation, Resources, Data curation, Writing – original draft, Writing – review & editing. **Vanderlan Nogueira Holanda:** Methodology, Formal analysis, Data curation. **Gabriela**

Plautz Ratkovski: Methodology, Formal analysis, Data curation. **Welson Vicente da Silva:** Investigation, Resources. **Pedro Henrique do Nascimento:** Investigation, Resources. **Regina Célia Bressan Queiroz de Figueiredo:** Conceptualization, Writing – original draft, Writing – review & editing, Supervision. **Celso Pinto de Melo:** Conceptualization, Writing – original draft, Writing – review & editing, Supervision, Project administration, Funding acquisition.

Declaration of competing interest

On behalf of all authors, I hereby certify that there is no conflict of interests in the publication of the manuscript "A new biocompatible silver/polypyrrole composite with in vitro antitumor activity", by Elton Marlon de Araújo Lima, Vanderlan Nogueira Holanda, Gabriela Plautz Ratkovski, Welson Vicente da Silva, Pedro Henrique do Nascimento, Regina Celia Bressan Queiroz de Figueiredo, and Celso Pinto de Melo, as no author has any financial/personal interest or belief, dual commitments, competing interests, or competing loyalties that could the corresponding work.

Acknowledgments

This work was supported by Brazilian agencies: FACEPE (Fundo de Amparo à Ciência e Tecnologia de Pernambuco, Brazil - IBPG-1510-3.03/16), CNPq (Conselho Nacional de Desenvolvimento Científico e Tecnológico, Brazil) and CAPES (Coordenação de Aperfeiçoamento de Pessoal de Nível Superior). The authors would like to thank Professor C. A. S. Andrade (Departamento de Bioquímica - Universidade Federal de Pernambuco) for the support on synthesis of composite, Professor C. F. Pereira (Departamento de Química Fundamental - Universidade Federal de Pernambuco) for the support on factorial analyses, and the Instituto Aggeu Magalhães for the use of the electron microscopy facility.

Appendix A. Supplementary data

Supplementary data to this article can be found online at https://doi.org/10.1016/j.msec.2021.112314.

References

[1] N.K. Guimard, N. Gomez, C.E. Schmidt, Prog. Polym. Sci. 32 (2007) 876–921, https://doi.org/10.1016/j.progpolymsci.2007.05.012.
[2] H. Shirakawa, E.J. Louis, A.G. MacDiarmid, C.K. Chiang, A.J. Heeger, J. Chem. Soc. Chem. Commun. (1977) 578–580, https://doi.org/10.1039/C39770000578.
[3] B. Liu Kenry, Biomacromolecules 19 (2018) 1783–1803, https://doi.org/10.1021/acs.biomac.8b00275.
[4] C.K. Chiang, C.R. Fincher, Y.W. Park, A.J. Heeger, H. Shirakawa, E.J. Louis, S. C. Gau, A.G. MacDiarmid, Phys. Rev. Lett. 39 (1977) 1098–1101, https://doi.org/10.1103/PhysRevLett.39.1098.
[5] M. Delvaux, J. Duchet, P.-Y. Stavaux, R. Legras, S. Demoustier-Champagne, Synth. Met. 113 (2000) 275–280, https://doi.org/10.1016/S0379-6779(00)00226-5.
[6] A.G. MacDiarmid, R.J. Mammone, R.B. Kaner, L. Porter, R. Pethig, A.J. Heeger, D. R. Rosseinsky, R.J. Gillespie, P. Day, Philos. Trans. R. Soc. Lond. A Math. Phys. Sci. 314 (1985) 3–15, https://doi.org/10.1098/rsta.1985.0004.
[7] Z. Zha, X. Yue, Q. Ren, Z. Dai, Adv. Mater. 25 (2013) 777–782, https://doi.org/10.1002/adma.201202211.
[8] R. Balint, N.J. Cassidy, S.H. Cartmell, Acta Biomater. 10 (2014) 2341–2353, https://doi.org/10.1016/j.actbio.2014.02.015.
[9] B.S. Dakshayini, K.R. Reddy, A. Mishra, N.P. Shetti, S.J. Malode, S. Basu, S. Naveen, A.V. Raghu, Microchem. J. 147 (2019) 7–24, https://doi.org/10.1016/j.microc.2019.02.061.
[10] S. Li, X. Shen, Q.-H. Xu, Y. Cao, Nanoscale 11 (2019) 19551–19560, https://doi.org/10.1039/C9NR05488J.
[11] A.P. O'Mullane, S.E. Dale, J.V. Macpherson, P.R. Unwin, Chem. Commun. (2004) 1606–1607, https://doi.org/10.1039/B404636F.
[12] D. Uppalapati, B.J. Boyd, S. Garg, J. Travas-Sejdic, D. Svirskis, Biomaterials 111 (2016) 149–162, https://doi.org/10.1016/j.biomaterials.2016.09.021.
[13] M. Cui, Z. Song, Y. Wu, B. Guo, X. Fan, X. Luo, Biosens. Bioelectron. 79 (2016) 736–741, https://doi.org/10.1016/j.bios.2015.12.101.
[14] R.J. da Silva, B.G. Maciel, J.C. Medina-Llamas, A.E. Chávez-Guajardo, J. J. Alcaraz-Espinoza, C. Pinto de Melo, Anal. Biochem. 575 (2019) 27–35, https://doi.org/10.1016/j.ab.2019.03.013.
[15] L. Han, Y. Zhang, Y. Zhang, Y. Shu, X.-W. Chen, J.-H. Wang, Talanta 171 (2017) 32–38, https://doi.org/10.1016/j.talanta.2017.04.056.
[16] J. Stejskal, Chem. Pap. 67 (2013) 814–848, https://doi.org/10.2478/s11696-012-0304-6.
[17] T.Y. Tekbaşoğlu, T. Soganci, M. Ak, A. Koca, M.K. Şener, Biosens. Bioelectron. 87 (2017) 81–88, https://doi.org/10.1016/j.bios.2016.08.020.
[18] S. Ye, S. Chen, H. Wang, Y. Lu, Phys. Chem. Chem. Phys. 13 (2011) 4668–4673, https://doi.org/10.1039/C0CP02184A.
[19] F. Zor, F.N. Selek, G. Orlando, D.F. Williams, Nanomedicine 14 (2019) 2763–2775, https://doi.org/10.2217/nnm-2019-0140.
[20] P. Humpolíček, V. Kašpárková, J. Pacherník, J. Stejskal, P. Bober, Z. Capáková, K. A. Radaszkiewicz, I. Junkar, M. Lehocký, Mater. Sci. Eng. C 91 (2018) 303–310, https://doi.org/10.1016/j.msec.2018.05.037.
[21] M. Ziąbka, M. Dziadek, E. Menaszek, Polymers 10 (2018) 1257, https://doi.org/10.3390/polym10111257.
[22] X. Wang, X. Gu, C. Yuan, S. Chen, P. Zhang, T. Zhang, J. Yao, F. Chen, G. Chen, J. Biomed. Mater. Res. A 68A (2004) 411–422, https://doi.org/10.1002/jbm.a.20065.
[23] A. Ramanavicius, A. Finkelsteinas, H. Cesiulis, A. Ramanaviciene, Bioelectrochemistry 79 (2010) 11–16, https://doi.org/10.1016/j.bioelechem.2009.09.013.
[24] U.T. Khatoon, G.V.S.N. Rao, M.K. Mohan, A. Ramanaviciene, A. Ramanavicius, J. Environ. Chem. Eng. 6 (2018) 5837–5844, https://doi.org/10.1016/j.jece.2018.08.009.
[25] U.T. Khatoon, G.V.S. Nageswara Rao, K.M. Mohan, A. Ramanaviciene, A. Ramanavicius, Vacuum 146 (2017) 259–265, https://doi.org/10.1016/j.vacuum.2017.10.003.
[26] L. Pauksch, S. Hartmann, M. Rohnke, G. Szalay, V. Alt, R. Schnettler, K.S. Lips, Acta Biomater. 10 (2014) 439–449, https://doi.org/10.1016/j.actbio.2013.09.037.
[27] M.J. Piao, K.A. Kang, I.K. Lee, H.S. Kim, S. Kim, J.Y. Choi, J. Choi, J.W. Hyun, Toxicol. Lett. 201 (2011) 92–100, https://doi.org/10.1016/j.toxlet.2010.12.010.
[28] S. Fujii, A. Aichi, K. Akamatsu, H. Nawafune, Y. Nakamura, J. Mater. Chem. 17 (2007) 3777–3779, https://doi.org/10.1039/B709413B.
[29] U. Mandi, S.K. Kundu, N. Salam, A. Bhaumik, S.M. Islam, J. Colloid Interface Sci. 467 (2016) 291–299, https://doi.org/10.1016/j.jcis.2016.01.017.
[30] F.J. Rodríguez, S. Gutiérrez, J.G. Ibanez, J.L. Bravo, N. Batina, Environ. Sci. Technol. 34 (2000) 2018–2023, https://doi.org/10.1021/es990940n.
[31] K. Firoz Babu, P. Dhandapani, S. Maruthamuthu, M. Anbu Kulandainathan, Carbohydr. Polym. 90 (2012) 1557–1563, https://doi.org/10.1016/j.carbpol.2012.07.030.
[32] N. Maráková, P. Humpolíček, V. Kašpárková, Z. Capáková, L. Martinková, P. Bober, M. Trchová, J. Stejskal, Appl. Surf. Sci. 396 (2017) 169–176, https://doi.org/10.1016/j.apsusc.2016.11.024.
[33] X. Tan, J. Wang, X. Pang, L. Liu, Q. Sun, Q. You, F. Tan, N. Li, ACS Appl. Mater. Interfaces 8 (2016) 34991–35003, https://doi.org/10.1021/acsami.6b11262.
[34] R.F.S. Santos, C.A.S. Andrade, C.G. dos Santos, C.P. de Melo, J. Nanopart. Res. 15 (2013) 1408, https://doi.org/10.1007/s11051-012-1408-1.
[35] P. Santa-Cruz, F. Teles, Ponto Quântico Nanodispositivos/RENAMI, 2003.
[36] J.P. Oliveira, A.R. Prado, W.J. Keijok, M.R.N. Ribeiro, M.J. Pontes, B.V. Nogueira, M.C.C. Guimarães, Arab. J. Chem. 13 (2020) 216–226, https://doi.org/10.1016/j.arabjc.2017.04.003.
[37] A.L. de Pinho Neves, C.C. Milioli, L. Müller, H.G. Riella, N.C. Kuhnen, H. K. Stulzer, Colloids Surf. A Physicochem. Eng. Asp. 445 (2014) 34–39, https://doi.org/10.1016/j.colsurfa.2013.12.058.
[38] L. Wilkinson, Am. Stat. 60 (2006) 332–334, https://doi.org/10.1198/000313006X152243.
[39] Z.-G. Yang, H.-X. Sun, W.-H. Fang, Vaccine 23 (2005) 5196–5203, https://doi.org/10.1016/j.vaccine.2005.06.016.
[40] L.V.F. Oliveira, F.F. Camilo, Synth. Met. 247 (2019) 219–227, https://doi.org/10.1016/j.synthmet.2018.12.001.
[41] W. Caseri, Macromol. Rapid Commun. 21 (2000) 705–722, https://doi.org/10.1002/1521-3927(20000701)21:11<705::AID-MARC705>3.0.CO;2-3.
[42] S. Jing, S. Xing, L. Yu, C. Zhao, Mater. Lett. 61 (2007) 4528–4530, https://doi.org/10.1016/j.matlet.2007.02.045.
[43] Y. Tan, K. Ghandi, Synth. Met. 175 (2013) 183–191, https://doi.org/10.1016/j.synthmet.2013.05.014.
[44] A. Xie, K. Zhang, M. Sun, Y. Xia, F. Wu, Mater. Des. 154 (2018) 192–202, https://doi.org/10.1016/j.matdes.2018.05.039.
[45] S.A.H. Jalali, A.R. Allafchian, S.S. Banifatemi, I. Ashrafi Tamai, J. Taiwan Inst. Chem. Eng. 66 (2016) 357–362, https://doi.org/10.1016/j.jtice.2016.06.011.
[46] J.D. Kim, H. Yun, G.C. Kim, C.W. Lee, H.C. Choi, Appl. Surf. Sci. 283 (2013) 227–233, https://doi.org/10.1016/j.apsusc.2013.06.086.
[47] B. Dong, M. Yang, S. Ge, Y. Cao, B. Li, Y. Lu, RSC Adv. 6 (2016) 23737–23745, https://doi.org/10.1039/C6RA01468B.
[48] A. Ramanavicius, V. Karabanovas, A. Ramanaviciene, R. Rotomskis, J. Nanosci. Nanotechnol. 9 (2009) 1909–1915, https://doi.org/10.1166/jnn.2009.361.
[49] K. Jia, P. Wang, L. Yuan, X. Zhou, W. Chen, X. Liu, J. Mater. Chem. C 3 (2015) 3522–3529, https://doi.org/10.1039/C4TC02850C.
[50] D. Muñoz-Rojas, J. Oró-Solé, O. Ayyad, P. Gómez-Romero, J. Mater. Chem. 21 (2011) 2078–2086, https://doi.org/10.1039/C0JM01449D.
[51] M.K. Rasmussen, J.N. Pedersen, R. Marie, Nat. Commun. 11 (2020) 2337, https://doi.org/10.1038/s41467-020-15889-3.
[52] J. Wen, Y. Tian, Z. Mei, W. Wu, Y. Tian, RSC Adv. 7 (2017) 53219–53225, https://doi.org/10.1039/C7RA09725E.

[53] Y.-C. Liu, T.C. Chuang, J. Phys. Chem. B 107 (2003) 12383–12386, https://doi.org/10.1021/jp035680h.
[54] B.C. Sih, M.O. Wolf, Chem. Commun. (2005) 3375–3384, https://doi.org/10.1039/B501448D.
[55] J.C. Gustafsson, B. Liedberg, O. Inganäs, Solid State Ionics 69 (1994) 145–152, https://doi.org/10.1016/0167-2738(94)90403-0.
[56] J. Xu, J. Hu, B. Quan, Z. Wei, Macromol. Rapid Commun. 30 (2009) 936–940, https://doi.org/10.1002/marc.200800764.
[57] P. Dallas, D. Niarchos, D. Vrbanic, N. Boukos, S. Pejovnik, C. Trapalis, D. Petridis, Polymer 48 (2007) 2007–2013, https://doi.org/10.1016/j.polymer.2007.01.058.
[58] H.V.R. Dias, M. Fianchini, R.M.G. Rajapakse, Polymer 47 (2006) 7349–7354, https://doi.org/10.1016/j.polymer.2006.08.033.
[59] S. Xing, G. Zhao, Mater. Lett. 61 (2007) 2040–2044, https://doi.org/10.1016/j.matlet.2006.08.011.
[60] R. Kostić, D. Raković, S.A. Stepanyan, I.E. Davidova, L.A. Gribov, J. Chem. Phys. 102 (1995) 3104–3109, https://doi.org/10.1063/1.468620.
[61] X. Feng, H. Huang, Q. Ye, J.-J. Zhu, W. Hou, J. Phys. Chem. C 111 (2007) 8463–8468, https://doi.org/10.1021/jp071140z.
[62] K.H. Kate, S.R. Damkale, P. Khanna, G. Jain, J. Nanosci. Nanotechnol. 11 (2011) 7863–7869, https://doi.org/10.1166/jnn.2011.4708.
[63] S. Kim, W.-K. Oh, Y.S. Jeong, J.-Y. Hong, B.-R. Cho, J.-S. Hahn, J. Jang, Biomaterials 32 (2011) 2342–2350, https://doi.org/10.1016/j.biomaterials.2010.11.080.
[64] S. Basu, A. Ghosh, A. Barui, B. Basu, J. Biomater. Appl. 33 (2019) 1035–1052, https://doi.org/10.1177/0885328218821549.
[65] J.E. Rayahin, R.A. Gemeinhart, Activation of macrophages in response to biomaterials, in: M. Kloc (Ed.), Macrophages: Origin, Functions and Biointervention, Springer International Publishing, Cham, 2017, pp. 317–351, https://doi.org/10.1007/978-3-319-54090-0_13.
[66] A. Nardin, J.-P. Abastado, Front. Biosci. 13 (2008) 494–505, https://doi.org/10.2741/2944.
[67] C. Du, A. Wang, J. Fei, J. Zhao, J. Li, J. Mater. Chem. B 3 (2015) 4539–4545, https://doi.org/10.1039/C5TB00560D.
[68] M. Mîndroiu, C. Ungureanu, R. Ion, C. Pîrvu, Appl. Surf. Sci. 276 (2013) 401–410, https://doi.org/10.1016/j.apsusc.2013.03.107.
[69] A. Ramanaviciene, A. Kausaite, S. Tautkus, A. Ramanavicius, J. Pharm. Pharmacol. 59 (2007) 311–315, https://doi.org/10.1211/jpp.59.2.0017.
[70] A. Vaitkuviene, V. Ratautaite, L. Mikoliunaite, V. Kaseta, G. Ramanauskaite, G. Biziuleviciene, A. Ramanaviciene, A. Ramanavicius, Colloids Surf. A Physicochem. Eng. Asp. 442 (2014) 152–156, https://doi.org/10.1016/j.colsurfa.2013.06.030.
[71] J.Y. Lee, C.E. Schmidt, J. Biomed. Mater. Res. A 103 (2015) 2126–2132, https://doi.org/10.1002/jbm.a.35344.
[72] A. Vaitkuviene, V. Kaseta, J. Voronovic, G. Ramanauskaite, G. Biziuleviciene, A. Ramanaviciene, A. Ramanavicius, J. Hazard. Mater. 250-251 (2013) 167–174, https://doi.org/10.1016/j.jhazmat.2013.01.038.
[73] Y. Chen, S. Xiang, L. Wang, M. Wang, C. Wang, S. Liu, K. Zhang, B. Yang, ChemPlusChem 83 (2018) 1127–1134, https://doi.org/10.1002/cplu.201800430.
[74] C.-g. Qian, Y.-l. Chen, P.-j. Feng, X.-z. Xiao, M. Dong, J.-c. Yu, Q.-y. Hu, Q.-d. Shen, Z. Gu, Acta Pharmacol. Sin. 38 (2017) 764–781, https://doi.org/10.1038/aps.2017.42.
[75] B. Tian, C. Wang, S. Zhang, L. Feng, Z. Liu, ACS Nano 5 (2011) 7000–7009, https://doi.org/10.1021/nn201560b.
[76] S. Häußler, M. Rohde, N. von Neuhoff, M. Nimtz, I. Steinmetz, Infect. Immun. 71 (2003) 2970, https://doi.org/10.1128/IAI.71.5.2970-2975.2003.
[77] J. Lam, M. Herant, M. Dembo, V. Heinrich, Biophys. J. 96 (2009) 248–254, https://doi.org/10.1529/biophysj.108.139154.
[78] H.R. Petty, D.G. Hafeman, H.M. McConnell, J. Cell Biol. 89 (1981) 223–229, https://doi.org/10.1083/jcb.89.2.223.
[79] K.R. Porter, V. Fonte, G. Weiss, Cancer Res. 34 (1974) 1385.
[80] J. Hardie, J.A. Mas-Rosario, S. Ha, E.M. Rizzo, M.E. Farkas, Pharmacol. Res. 148 (2019), 104452, https://doi.org/10.1016/j.phrs.2019.104452.
[81] H.M. Rostam, P.M. Reynolds, M.R. Alexander, N. Gadegaard, A. M. Ghaemmaghami, Sci. Rep. 7 (2017) 3521, https://doi.org/10.1038/s41598-017-03780-z.
[82] S.-R. Kang, D.-Y. Han, K.-I. Park, H.-S. Park, Y.-B. Cho, H.-J. Lee, W.-S. Lee, C. H. Ryu, Y.L. Ha, D.H. Lee, Evid. Based Complement. Alternat. Med. 2011 (2011), https://doi.org/10.1155/2011/248592.
[83] M. Gniadek, A. Wichowska, M. Antos-Bielska, P. Orlowski, M. Krzyzowska, M. Donten, Synth. Met. 266 (2020), 116430, https://doi.org/10.1016/j.synthmet.2020.116430.
[84] R.G.D. Andrade, B. Reis, B. Costas, S.A.C. Lima, S. Reis, Polymers 13 (2021) 88, https://doi.org/10.3390/polym13010088.
[85] L.A.B. Ferreira, F. Garcia-Fossa, A. Radaic, N. Durán, W.J. Fávaro, M.B. de Jesus, Eur. J. Pharm. Biopharm. 151 (2020) 162–170, https://doi.org/10.1016/j.ejpb.2020.04.012.
[86] M.C. Stensberg, Q. Wei, E.S. McLamore, D.M. Porterfield, A. Wei, M.S. Sepúlveda, Nanomedicine 6 (2011) 879–898, https://doi.org/10.2217/nnm.11.78.
[87] J. Wang, J. Yi, Cancer Biol. Ther. 7 (2008) 1875–1884, https://doi.org/10.4161/cbt.7.12.7067.
[88] C.R. Reczek, N.S. Chandel, Annu. Rev. Cancer Biol. 1 (2017) 79–98, https://doi.org/10.1146/annurev-cancerbio-041916-065808.
[89] Q. Zou, J. Huang, X. Zhang, Small 14 (2018), 1803101, https://doi.org/10.1002/smll.201803101.
[90] S. Henkelman, G. Rakhorst, J. Blanton, W. van Oeveren, Mater. Sci. Eng. C, 29 (2009) 1650–1654, https://doi.org/10.1016/j.msec.2009.01.002.
[91] J. Upadhyay, A. Kumar, B. Gogoi, A.K. Buragohain, Mater. Sci. Eng. C 54 (2015) 8–13, https://doi.org/10.1016/j.msec.2015.04.027.
[92] K.C. Barick, P.A. Hassan, J. Colloid Interface Sci. 369 (2012) 96–102, https://doi.org/10.1016/j.jcis.2011.12.008.
[93] D. Xiong, Y. Deng, N. Wang, Y. Yang, Appl. Surf. Sci. 298 (2014) 56–61, https://doi.org/10.1016/j.apsusc.2014.01.088.
[94] E. Hosoi, J. Med. Investig. 55 (2008) 174–182, https://doi.org/10.2152/jmi.55.174.
[95] J. Choi, V. Reipa, V.M. Hitchins, P.L. Goering, R.A. Malinauskas, Toxicol. Sci. 123 (2011) 133–143, https://doi.org/10.1093/toxsci/kfr149.
[96] L. Tavano, M.R. Infante, M.A. Riya, A. Pinazo, M.P. Vinardell, M. Mitjans, M. A. Manresa, L. Perez, Soft Matter 9 (2013) 306–319, https://doi.org/10.1039/C2SM26670A.
[97] W.-S. Cho, R. Duffin, F. Thielbeer, M. Bradley, I.L. Megson, W. MacNee, C. A. Poland, C.L. Tran, K. Donaldson, Toxicol. Sci. 126 (2012) 469–477, https://doi.org/10.1093/toxsci/kfs006.
[98] C. McGuinnes, R. Duffin, S. Brown, N.L. Mills, I.L. Megson, W. MacNee, S. Johnston, S.L. Lu, L. Tran, R. Li, X. Wang, D.E. Newby, K. Donaldson, Toxicol. Sci. 119 (2010) 359–368, https://doi.org/10.1093/toxsci/kfq349.
[99] F. Tokumasu, G.R. Ostera, C. Amaratunga, R.M. Fairhurst, Exp. Parasitol. 131 (2012) 245–251, https://doi.org/10.1016/j.exppara.2012.03.005.
[100] T.J. Jayeoye, O.F. Nwabor, T. Rujiralai, J. Ind. Eng. Chem. 89 (2020) 288–300, https://doi.org/10.1016/j.jiec.2020.05.025.
[101] Z. Lu, X. Zhang, Z. Li, Z. Wu, J. Song, C. Li, Polym. Chem. 6 (2015) 772–779, https://doi.org/10.1039/C4PY00931B.